J. Biochem. 2011;149(1):67–74 doi:10.1093/jb/mvq117

JB THE JOURNAL OF BIOCHEMISTRY

Visualization of polymorphism in apolipoprotein C-II amyloid fibrils

Received August 29, 2010; accepted September 25, 2010; published online September 30, 2010

Chai L. Teoh[1], Hisashi Yagi[2], Michael D.W. Griffin[1], Yuji Goto[2] and Geoffrey J. Howlett[1,*]

[1]Department of Biochemistry and Molecular Biology, Bio21 Molecular Science and Biotechnology Institute, University of Melbourne, Parkville, Victoria 3010, Australia; and [2]Institute for Protein Research, Osaka University, 3-2 Yamadaoka, Suita, Osaka 565-0871, Japan

*Geoffrey J. Howlett, Department of Biochemistry and Molecular Biology, Bio21 Molecular Science and Biotechnology Institute, The University of Melbourne, 30 Flemington Road, Parkville, Victoria, 3010, Australia. Tel: +61 3 8344 2271, Fax: +61 3 9348 1421, email: ghowlett@unimelb.edu.au

The misfolding and self-assembly of proteins into amyloid fibrils, which occur in several debilitating and age-related diseases, are affected by common components of amyloid deposits, notably lipids and lipid complexes. Previously, the effects of phospholipids on amyloid fibril formation by apolipoprotein (apo) C-II have been examined, where low concentrations of micellar phospholipids and lipid bilayers induce a new, straight rod-like morphology for apoC-II fibrils. This fibril appearance is distinct from the twisted-ribbon morphology observed when apoC-II fibrils are formed in the absence of lipids. We used total internal reflection fluorescence microscopy (TIRFM) to visualize the described polymorphism of apoC-II amyloid fibrils. The spontaneous assembly of apoC-II into either twisted-ribbon fibrils in the absence of lipids or into fibrils of straight rod-like morphology when lipids are present was captured by TIRFM. The latter was found to be better suited for visualization using TIRFM. The difference between seeding of apoC-II straight fibrils on microscopic quartz slide and in test tube suggested a role for the effects of incubation surface on fibril formation. Seed-dependent growth of apoC-II straight fibrils was probed further by using a dual-labelling construct, giving insights into the straight fibril growth pattern.

Keywords: amyloid fibrils/apolipoprotein C-II/fluorescence microscopy/lipids/morphology.

Abbreviations: AFM, atomic force microscopy; apo, apolipoprotein; DHPC, dihexanoylphosphatidylcholine; GuHCl, guanidine hydrochloride; IAPP, islet amyloid polypeptide; LysoMPC, 1-myristoyl-2-hydroxy-*sn*-glycero-3-phosphocholine; TEM, transmission electron microscopy; ThT, thioflavin T; TIRFM, total internal reflection fluorescence microscopy.

Current interest in the structure and assembly mechanisms for amyloid fibrils stems from their association with a wide range of debilitating diseases (*1–3*). Each disease is characterized by a particular protein or polypeptide, which misfolds and aggregates into highly ordered protein polymers that share a number of common properties. To date, more than 25 proteins are known to self-assemble into amyloid fibrils *in vivo* with subsequent accumulation of these structures, either intra- or extra-cellularly, ultimately resulting in the development of disease. A common feature in many of the most important and prominent amyloid forming proteins is their ability to bind lipids and lipid complexes (*3*). Some examples of the lipid-binding proteins that form amyloid *in vivo* include Aβ, which accumulates in Alzheimer's disease (*4*) and the islet amyloid polypeptide (IAPP), which accumulates as insoluble polymers in the pancreas of individuals with type 2 diabetes (*5*, *6*).

Our work focuses on another lipid-binding protein that readily forms amyloid fibrils, apolipoprotein (apo) C-II, which is one of several members of the apo family that accumulate in atherosclerotic plaques (*7*). Human apoC-II is a 79 amino acid co-factor of the lipid rich very low-density lipoproteins and chylomicrons, which transport lipids through the bloodstream. Under lipid-free conditions *in vitro*, apoC-II spontaneously aggregates to form homogenous amyloid fibrils with all the hallmarks of amyloid fibrils (*8*), including fibrous morphology, the ability to interact with Congo Red and Thioflavin T (ThT) and cross-β structure as shown by X-ray diffraction (*9*). ApoC-II fibrils are relatively homogenous in structure and form readily under quiescent conditions. This allows extensive characterization of amyloid fibril formation by apoC-II, including the parameters that control fibril formation. Analysis of the rate of apoC-II fibril formation and their size distribution at different concentrations has led to the development of a detailed kinetic model for apoC-II fibril formation, involving reversible nucleation–elongation process coupled with fibril breaking and rejoining (*10*).

Phospholipids exert significant effects on apoC-II fibril formation. While high concentrations of micellar lipids stabilize α-helical structures and prevent fibril formation (*11*), submicellar phospholipids and oxidized cholesterol derivatives accelerate amyloid fibril formation (*12*). Our previous work shows that submicellar dihexanoylphosphatidylcholine (DHPC) activation of apoC-II fibril formation occurs by promoting the rapid formation of a tetrameric species

followed by a slow isomerization that precedes monomer addition and fibril growth (*13*). Our studies also support the distinct nature of nucleation and elongation, demonstrating that submicellar DHPC promotes the nucleation of apoC-II fibrils without significantly affecting the rate of fibril elongation or the rate of fibril breaking and joining (*14*). In contrast, low concentrations of micellar phospholipids and lipid bilayers, while initially inhibiting fibril formation, will ultimately induce a novel, straight rod-like morphology for apoC-II fibrils (*11*), which is distinct from the twisted-ribbon morphology usually observed for apoC-II fibrils formed in the absence of lipids (*8*).

These studies with apoC-II show that phospholipid complexes can change the structural architecture of mature fibrils and generate new morphologies with the potential to alter the *in vivo* behaviour of amyloid. Knowledge of the molecular structure and formation of amyloid fibrils is essential for understanding the pathology of amyloid diseases and will promote the development of treatment strategies. Most morphological investigations of amyloid fibrils have been performed with transmission electron microscopy (TEM) (*15*, *16*), while atomic force microscopy (AFM) has become a major method in the past few years (*17–19*).

More recently, the development of total internal reflection fluorescence microscopy (TIRFM) using ThT fluorescence has been successfully applied to the direct observation of fibril growth at the single fibril level to yield essential information about the mechanism of fibrillation (*20–27*). In this article, we report the first application of TIRFM towards the visualization of the described polymorphism in apoC-II fibrils.

Materials and Methods

Materials

Human apoC-II was expressed and purified as described previously (*11*). Purified apoC-II stocks were maintained in 5 M GuHCl, 10 mM Tris–HCl, pH 8.0 at a concentration of ~40 mg/ml. ApoC-II$_{S11C}$ conjugated with Alexa 488 dye as described previously (*13*) was provided by Dr Tim Ryan (University of Melbourne). 1-myristoyl-2-hydroxy-*sn*-glycero-3-phosphocholine (LysoMPC) was acquired from Avanti Polar Lipids (AL, USA) and was stored in chloroform at −20°C. All reagents were of analytical grade specification.

Preparation of phospholipids

Aqueous solutions of lipids were prepared by initial drying of chloroform stocks under nitrogen followed by complete drying *in vacuo* overnight. The dried lipid was rehydrated in 100 mM sodium phosphate buffer (pH 7.4) containing 0.1% sodium azide, to the desired concentration of 50 mM and mixed thoroughly.

Fibril formation and isolation of straight fibrils

Fibril formation was initiated by diluting apoC-II stocks to the desired protein concentration in 100 mM sodium phosphate buffer (pH 7.4) containing 0.1% sodium azide. Fibril formation was conducted at room temperature (25°C). In the case of straight-type fibrils, formation was initiated at 1.0 mg/ml (112 μM) apoC-II in the presence of 500 μM LysoMPC.

The rapid sedimentation of the straight-type fibrils facilitated relatively simple isolation of these from both the ribbon-type fibrils and the bulk lipid in solution. Straight fibrils formed at 1.0 mg/ml (112 μM) apoC-II in the presence of 500 μM LysoMPC were centrifuged for 2 min at 14,500*g* and the supernate removed. The resulting fibril pellet was re-suspended in an equal volume of 100 mM sodium phosphate, pH 7.4 and the process repeated for a total of three times.

Fibril fragments used as seeds were prepared from isolated straight fibrils by freeze-thaw cycling. Small aliquots of fibrils were frozen with liquid nitrogen and allowed to thaw at room temperature. Five freeze-thaw cycles were employed.

Preparation of slides for TIRFM

Quartz slides were first cleaned with 0.5 % (v/v) Hellmanex (Hellma, Müllheim, Germany)/water and then treated with a solution of acetone for 30 min, rinsed extensively with distilled water and finally dried in a vacuum oven at 100°C before subjecting them to plasma generation.

TIRFM

The TIRFM system used to observe individual amyloid fibrils was developed based on an inverted microscope (IX70, Olympus, Tokyo, Japan) as described (*20–22*). ThT was excited at 442 nm (emission 480 nm) by a helium–cadmium laser (IK5552R-F, Kimmon, Tokyo, Japan), while the Alexa 488 was excited at 488 nm (emission 520 nm) by an argon laser (Spectra-Physics, Tokyo, Japan). The fluorescence image was filtered with a bandpass filter (ThT: D490/30, Omega Optical, Bratteboro, VT, Alexa488: D529/28, OPTO-LINE, Inc.) and visualized using a digital steel camera (DP70, Olympus).

Seeds of apoC-II prepared as described above were added at a final concentration of 0.03–1 mg/ml apoC-II in 100 mM sodium phosphate (pH 7.4) containing 0.1% sodium azide. ThT solution was then added at a final concentration of 20 μM. An aliquot (10 μl) of each sample solution was deposited on each microscopic quartz slide and an image of the fibrils was obtained with TIRFM. After the mixing of the solutions of seeds, monomeric proteins and ThT at the same final concentrations as above, the mixture was immediately deposited (14 μl) on the microscopic slide, tightly sealed with a coverslip and incubated at 25°C, or alternatively, left incubated in the sampling tube before being transferred to a microscopic slide (10 μl) for imaging.

AFM

A sample solution was spotted on a freshly cleaved mica. After standing for 1 min, the residual solution was blotted off. AFM images were acquired using a Digital Instruments NanoscopeIIIa scanning microscope at 25°C (Veeco, Tokyo, Japan). Measurements were performed in an air-tapping mode.

Results

Ribbon fibrils versus straight fibrils

A summary of the proposed assembly pathways leading to ribbon fibrils and straight fibrils is illustrated in Fig. 1. In the lipid-free state, apoC-II monomers readily self-associate into twisted-ribbon fibrils (Fig. 2B), possibly via a partially folded intermediate. Alternatively, soluble apoC-II can bind to lipid surfaces inducing α-helical structure and inhibiting fibril formation. Our previous study proposed that under limiting lipid conditions and extended incubation period, the rapid reversible binding of apoC-II to the lipid surface results in significant populations of both lipid-bound apoC-II and released protein in a lipid-bound-like conformation (*11*). Under these conditions, straight fibrils may either nucleate at the crowded lipid surface or assemble in solution from apoC-II in the lipid-bound-like conformation. Based on these findings and to extend our knowledge of apoC-II fibril structure and formation from previous microscopic analysis, we applied TIRFM to visualize the distinct fibril morphology produced by apoC-II under different environments. The approach using TIRFM and ThT can be applied to various amyloid fibrils since the binding of ThT is a common property of amyloid

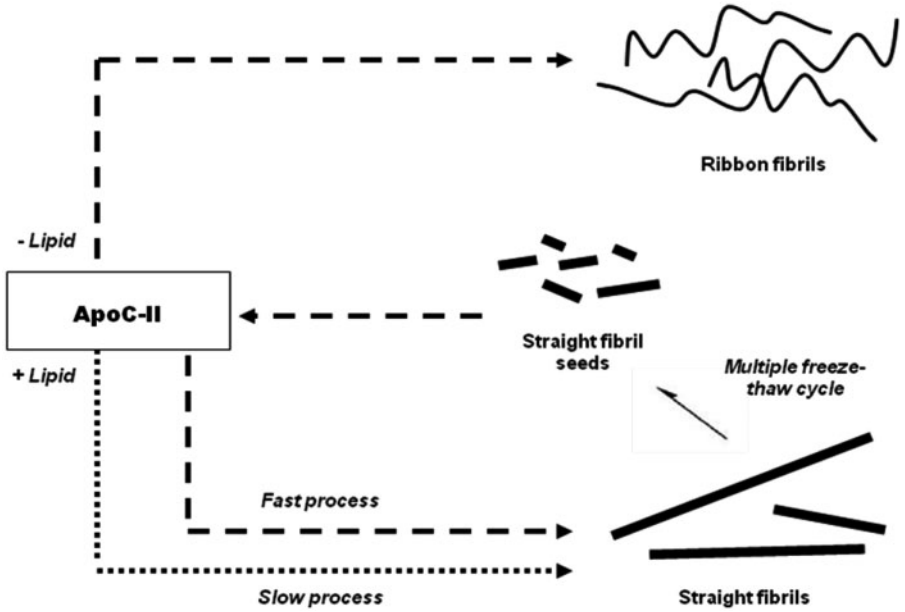

Fig. 1 Schematic summary of the proposed assembly pathways leading to ribbon-type fibrils and straight fibrils. Adapted from reference (*11*).

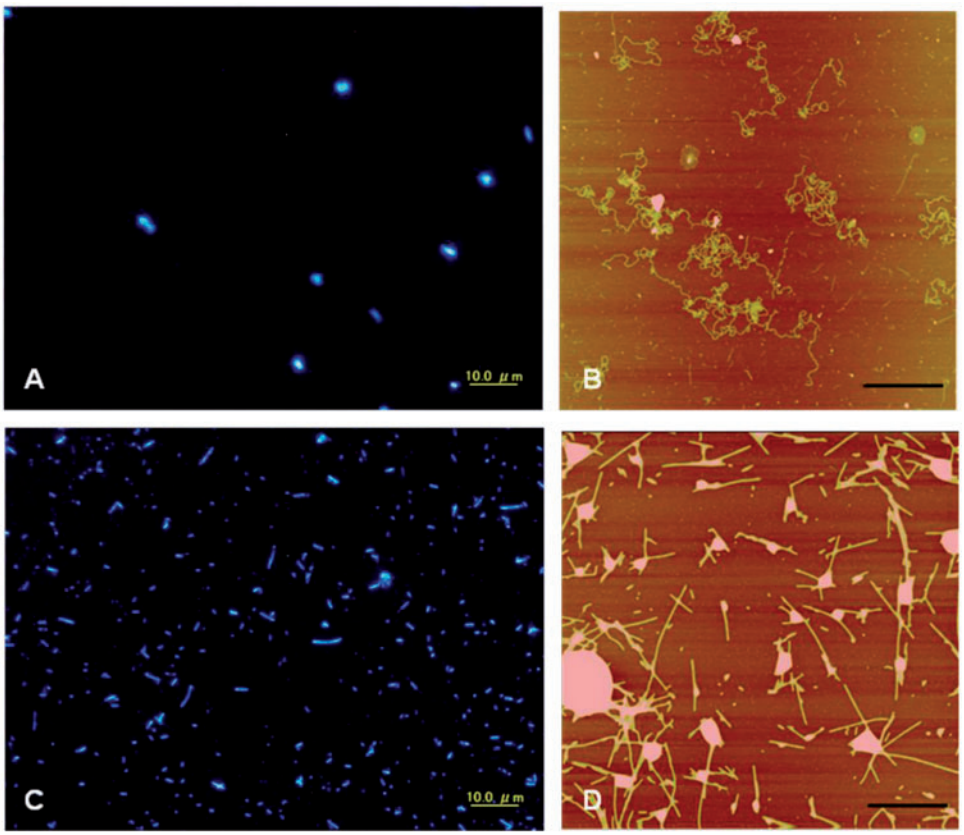

Fig. 2 Spontaneous formation of apoC-II amyloid fibrils in test tube. Ribbon-type fibrils are shown in (A and B) and straight-type fibrils grown in the presence of 500 μM LysoMPC are shown in the below figures. (A and C) were viewed by TIRFM. (B and D) were viewed by AFM. Scale bar for AFM images is 1 μm.

fibrils. As ThT is a reagent known to become strongly fluorescent upon binding to amyloid fibrils (*28*, *29*), one can observe the fibrils and the process by which they form without introducing any fluorescence reagent covalently bound to the protein molecule.

Self-assembly of apoC-II into amyloid fibrils with distinct morphologies in test tube

First, apoC-II ribbon fibrils were induced under similar conditions as reported previously (*11*). TIRFM of the sample (Fig. 2A) revealed only several bright

fluorescence spots, indicating the presence of ThT bound apoC-II fibrils, while the characteristic folding and curling of the standard ribbon-type fibril was not observed. However, when examined by AFM under ambient conditions, we could see the characteristic morphology of apoC-II fibrils, confirming the presence of tangled fibrils and some closed loop structures in the sample preparation (Fig. 2B), consistent with previous observations (*8*).

Second, straight fibrils of apoC-II were formed spontaneously in the presence of 500 μM LysoMPC at room temperature with occasional mixing and incubated for over 672 h. Under these conditions, fibrils of apoC-II exhibit a rigid rod-like appearance (*11*). Indeed, we observed a population of straight, rod-like structures of variable lengths by TIRFM (Fig. 2C). The same preparation when subjected to AFM analysis (Fig. 2D) confirmed the abundance of straight-type fibrils. In contrast to the ribbon-type fibrils, which are ~11–12 nm in width, these straight fibrils are ~13–14 nm in width and can be up to several micrometers in length (*11*). AFM also measured the fibrils to be ~7 nm in height, almost 3.5 times thicker than ribbon-type fibrils (data not shown).

Seed-dependent formation of straight fibrils on quartz surface and in test tube

Initial TIRFM analysis indicated apoC-II straight fibrils were better candidates for direct observation of fibril growth. However, to monitor fibril growth in real time at the single fibril level required fibrillation to take place on the quartz surface. As long incubation (>3 days) on the slide glass tends to dry the samples, making TIRFM experiments difficult, it was necessary to significantly shorten the incubation time required for straight-type fibril formation. Earlier seeding experiments showed that the rigid rod fibril structure of apoC-II could be seeded (Fig. 1) (*11*). Structural seeding using fragments prepared from isolated preformed straight fibrils by freeze thawing resulted in reduction or removal of the 'lag phase' for formation of straight fibrils. Previously, under lipid-free conditions in the presence of seeds, straight daughter fibrils were found to be abundant within 200 h incubation time. Fibril formation was strikingly faster, however, when seeded in the presence of lipid, yielding daughter straight fibrils after 24 h (*11*). Based on this previous knowledge, we attempted the accelerated growth of apoC-II straight fibrils in the presence of seeds and phospholipids on a quartz surface, to allow for closer investigation of this alternative fibril formation by TIRFM.

As described previously (*11*), apoC-II was incubated in the presence of 500 μM LysoMPC, 3% straight fibril seeds (relative to the total apoC-II concentration) and 20 μM ThT. An aliquot of the mixture was deposited onto the microscopic quartz slide and immediately observed by TIRFM ($t = 0$ day) before being subjected to further incubation at 25°C to allow for fibril formation. As a control, the remaining protein mixture which was not deposited on slide was left for incubation in the sampling tube under the same conditions until further analysis by TIRFM. Initial observation of sample preparation ($t = 0$ day), showed abundant fluorescence spots, indicating the presence of straight fibrils seeds (Fig. 3A). When monitored by TIRFM again at $t = 3$ days (Fig. 3B), the sample prepared and incubated on the quartz slide did not yield any significant changes in appearance. It appears that only ThT reactive spots were detected but none of them exhibited fibrillar morphology. In stark contrast, however, the same sample preparation that was incubated in the sample tube produced straight-type fibrils, as demonstrated in Fig. 3C. Further analysis by AFM (Fig. 3D) confirmed the presence of fibrils with rigid rod appearance with incidence of ribbon type fibrils, as reported previously (*11*). As a control, the same reaction mixture was prepared but without the addition of ThT in the sample tube. Similar observations were recorded when ThT is added immediately prior to TIRFM visualization (data not shown). Hence, it is unlikely that the inhibition of fibril extension on quartz slide is caused by ThT binding. These results suggest that the incubation surface of the quartz slide inhibits fibril extension compared with the solution environment of the test tube, although the exact mechanism for this effect is unknown.

ApoC-II straight fibril formation using Alexa 488-labelled seeds

A dual-labelling construct was used to gain more information and to further understand the seed-dependent formation of straight fibrils. This was accomplished by tagging seed fibrils covalently with a fluorescent dye (Alexa 488). The labelled seed fibrils were then added to a reaction mixture of unlabelled monomeric apoC-II in the presence of phospholipids and the elongated seed material was incubated with ThT. The entire fibrils are detected by ThT fluorescence emission, whereas the seeds are observed by fluorescence emission of Alexa 488, allowing the original fibril seeds to be observed in a grown fibril.

ApoC-II$_{S11C}$ conjugated with Alexa 488 (100% labelled) was induced to form straight fibrils under the same conditions as described earlier for wild-type apoC-II. Observation by TIRFM, as well as micrographs from AFM, both confirmed the presence of Alexa 488-labelled apoC-II$_{S11C}$ fibrils with a rigid rod-like appearance that emit bright green Alexa 488 fluorescence when excited (data not shown). Unlabelled apoC-II monomers were incubated in the buffer containing phospholipids and Alexa 488-labelled apoC-II$_{S11C}$ straight fibril fragments as seeds. The sample mixture in the test tube was transferred onto a quartz slide and ThT was added immediately before TIRFM observation. The TIRFM images were recorded by monitoring the emission of Alexa 488 and ThT fluorescence respectively, at the initiation of fibril formation ($t = 0$ day) and after 2-days incubation ($t = 2$ days). At $t = 0$, straight fibril seeds yielded bright green fluorescence when the Alexa 488 fluorophore was selectively excited (Fig. 4A). As expected, the Alexa 488-labelled straight fibril seeds were also detected by ThT (Fig. 4B). Figure 4C shows that both images (Fig. 4A and B) overlay well when merged. After 2-days incubation in the test tube,

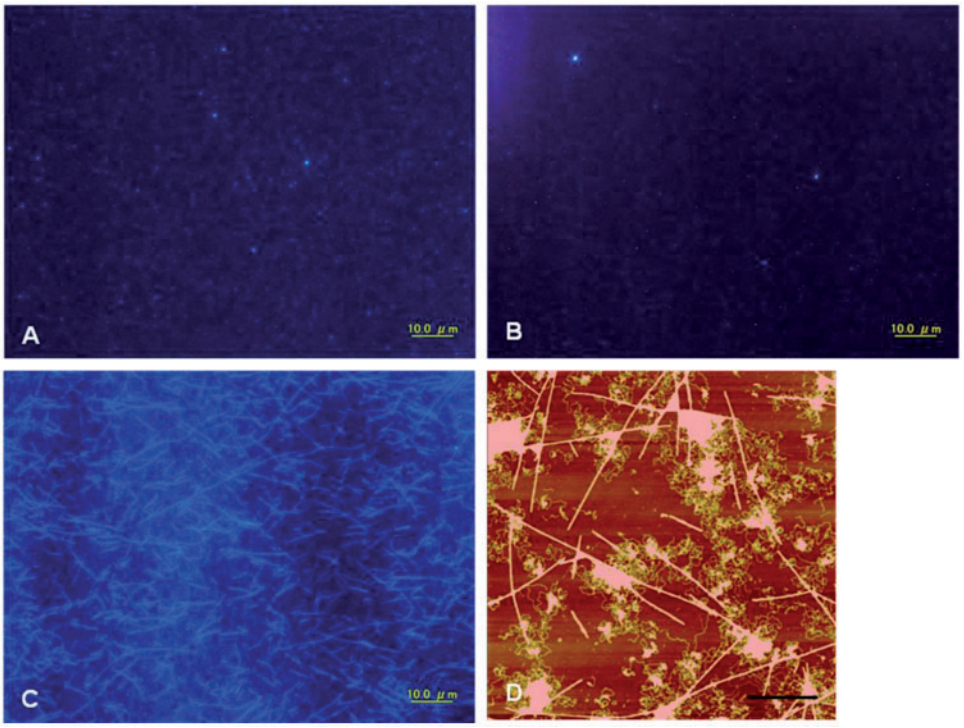

Fig. 3 Seed-dependent growth of apoC-II straight fibrils in the presence of phospholipids on quartz slide and in test tube. Straight fibrils were seeded in the presence of 500 μM LysoMPC on the quartz slide (A and B) and in the test tube (C and D). Samples were viewed by TIRFM at the start (A) and after 3 days incubation (B and C). Sample incubated for 3 days in test tube was also analysed by AFM (D). Scale bar for AFM images is 1 μm.

changes in the appearance of the sample were observed, indicating the growth of straight fibrils (Fig. 4D and E). Furthermore, clues on the seed-dependent formation of daughter straight fibrils could be revealed when images from ThT and Alexa 488 fluorescence emissions (Fig. 4D and E) were merged (Fig. 4F). While many of the straight-type fibrils seem to have formed in a rather spontaneous fashion, some examples were observed where the daughter straight fibrils extended from the parent seeds. Figure 4G provides closer examination of the merged figures.

Discussion

TEM and AFM techniques have commonly been used for morphological investigations of amyloid fibrils (*15–19*). Recently, the development of a technique which uses TIRFM combined with ThT fluorescence has been successfully applied to directly observe fibril growth (*20–25*, *27*). In this article, we show the application of TIRFM to visualize and study the formation of apoC-II amyloid fibrils and outline the limitations and the potentials of this technique. As anticipated, inspection of the fine structural details in apoC-II fibrils proved to be limited by TIRFM. This is largely due to the smaller size of apoC-II fibrils compared with amyloid fibrils formed by other proteins, which have been previously studied with the same detection system (*20–27*). Ribbon-like morphologies of Aβ-fibrils were observed with all of AFM, TEM and TIRFM under specified conditions (*24*), where the length and width were much larger than those of apoC-II fibrils. Here, although the ribbon-like morphology of apoC-II fibrils is evident from AFM images, TIRFM revealed only a large number of fluorescent spots of similar size. We consider that the shorter persistence length of apoC-II fibrils and its more flexible twisted morphology promoted tangling and clumping, thus giving rise only to fluorescence clusters when monitored by TIRFM. It is also likely that the rather soluble nature of apoC-II fibrils may have contributed to such an appearance. ApoC-II straight fibrils, on the other hand, which are larger and more rigid, were better suited for TIRFM observation, revealing clear images.

Previous studies used TIRFM to observe the seed-dependent elongation of fibrils in real-time and at a single fibril level (*20–23*, *26*). The seed-dependent reaction significantly shortens the lag-phase of fibril formation, while providing insights into the growth pattern since fibril elongation from the original seeds can be monitored over time. We found that seed-dependent growth of apoC-II under conditions favouring straight fibrils was inhibited when the sample was prepared and incubated on microscopic slides. Conversely, if seeding was initiated in solution, the formation of straight fibrils was confirmed by TIRFM. We propose that this difference in straight fibril formation is due to differences between the incubation surface of the quartz slide and the solution environment of the test tube. Under the conditions of TIRFM experiments, the reaction area is 18 mm × 18 mm and the distance between quartz slide and cover glass is 10 μm. It is possible that the narrow

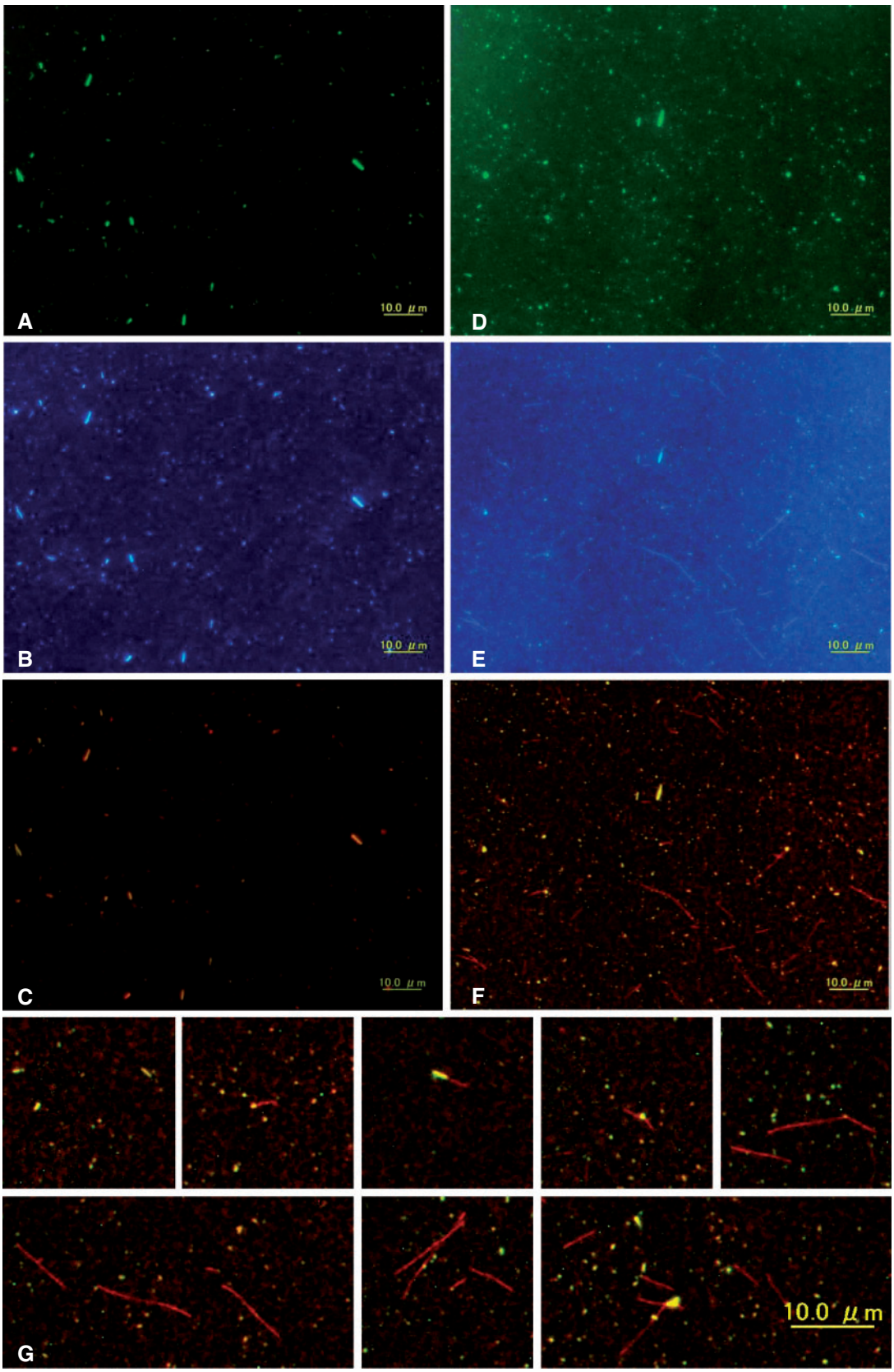

Fig. 4 Seed-dependent growth of apoC-II straight fibrils in the test tube. Straight fibrils were seeded in the presence of 500 μM LysoMPC using Alexa 488-labelled apoC-II$_{S11C}$ seeds. Samples were viewed by TIRFM (A–C) at the start and (D–F) after 2-days incubation. (A and D) show Alexa 488 fluorescence emission, whereas (B and E) show ThT fluorescence emission. C is a merged image of (A and B), while F is a merged image of (D and E). G shows detailed images from F.

reaction space may have inhibited fibril growth. Another likely explanation for the suppressed fibril formation is the immobilization of the fibril seeds on the surface of microscopic quartz slide, preventing elongation and subsequent fibril growth.

By using a dual-labelling construct, the original fibril seeds can be observed in a grown fibril. This provides an alternate method to observe fibril growth from a seed that is used to nucleate fibril formation. In this fashion, the mechanism of fibril elongation in solution can be better studied. As straight fibril formation is not complete during the observed time period, it is likely that by separating the twisted-ribbon fibrils from the straight ones using centrifugation prior to observation by TIRFM, the high background fluorescence in the images can be reduced. Most observations were that the elongated fibrils tend to be on one end of the seeds, suggesting that the fibril grows uni-directionally. However, in a few cases, fibrils appear to grow in both longitudinal directions. This added degree of uncertainty may arise when fibrils overlay on top of each other. Nonetheless, it is still apparent from the TIRFM images that not all seeds have fibril extended from them and where there are examples of fibril extension from the parent seed, the fibrils length appeared to be short. In most cases, the longer straight fibrils seem to be nucleated without the presence of an observed preformed seed. However, given the prolonged incubation time required for apoC-II to spontaneously assemble into straight fibrils, it is unlikely that the longer straight fibrils have been formed in a spontaneous fashion. A possible explanation for the absence of parent seed is that the longer fibrils have experienced fragmentation or breakage. Another possible explanation is that the seeded end of the fibril is out of the evanescent fields monitored by TIRFM. As the evanescent field formed by the total internal reflection of laser light penetrates to a depth of around 150 nm, only fluorophores located within this field will be detected. Thus, the full-length of a fibril can be observed only if fibrils are lying along the slide glass within the 150 nm range.

In conclusion, with TIRFM, we succeeded in visualizing the phospholipid-dependent polymorphism of apoC-II amyloid fibrils. The ability of one polypeptide to form aggregates of different morphologies and the ability of different polypeptides to grow into a common fibrillar amyloid morphology are important features of amyloid fibrils. Morphology of amyloid deposits can vary dramatically even for one protein depending on the tissue and disease conditions. The current results with apoC-II support our previous work that the interactions with phospholipid membranes are critical in determining the polymorphism (*11–13*). Further analysis with TIRFM in real time with improved resolution so as to visualize the details of ribbon-like fibrils will be a next step toward clarifying the phospholipid-dependent polymorphism of amyloid fibrils and their formation.

Acknowledgements

The authors thank Dr Danny Hatters for his suggestions on the preparation of figures.

Funding
Australian Research Council (DP0877800); Postgraduate Overseas Research Experience Scholarship (PORES) scheme of the University of Melbourne, Australia.

Conflict of interest
None declared.

References

1. Selkoe, D.J. (2003) Folding proteins in fatal ways. *Nature* **426**, 900–904
2. Chiti, F. and Dobson, C.M. (2006) Protein misfolding, functional amyloid, and human disease. *Annu. Rev. Biochem.* **75**, 333–366
3. Westermark, P., Benson, M.D., Buxbaum, J.N., Cohen, A.S., Frangione, B., Ikeda, S., Masters, C.L., Merlini, G., Saraiva, M.J., and Sipe, J.D. (2007) A primer of amyloid nomenclature. *Amyloid* **14**, 179–183
4. Matsuzaki, K. (2007) Physicochemical interactions of amyloid beta-peptide with lipid bilayers. *Biochim. Biophys. Acta* **1768**, 1935–1942
5. Kahn, S.E., Andrikopoulos, S., and Verchere, C.B. (1999) Islet amyloid: a long-recognized but underappreciated pathological feature of type 2 diabetes. *Diabetes* **48**, 241–253
6. Engel, M.F., Khemtemourian, L., Kleijer, C.C., Meeldijk, H.J., Jacobs, J., Verkleij, A.J., de Kruijff, B., Killian, J.A., and Hoppener, J.W. (2008) Membrane damage by human islet amyloid polypeptide through fibril growth at the membrane. *Proc. Natl Acad. Sci. USA* **105**, 6033–6038
7. Stewart, C.R., Haw, A. 3rd, Lopez, R., McDonald, T.O., Callaghan, J.M., McConville, M.J., Moore, K.J., Howlett, G.J., and O'Brien, K.D. (2007) Serum amyloid P colocalizes with apolipoproteins in human atheroma: functional implications. *J. Lipid Res.* **48**, 2162–2171
8. Hatters, D.M., MacPhee, C.E., Lawrence, L.J., Sawyer, W.H., and Howlett, G.J. (2000) Human apolipoprotein C-II forms twisted amyloid ribbons and closed loops. *Biochemistry* **39**, 8276–8283
9. Hatters, D.M., MacRaild, C.A., Daniels, R., Gosal, W.S., Thomson, N.H., Jones, J.A., Davis, J.J., MacPhee, C.E., Dobson, C.M., and Howlett, G.J. (2003) The circularization of amyloid fibrils formed by apolipoprotein C-II. *Biophys. J.* **85**, 3979–3990
10. Binger, K.J., Pham, C.L., Wilson, L.M., Bailey, M.F., Lawrence, L.J., Schuck, P., and Howlett, G.J. (2008) Apolipoprotein C-II amyloid fibrils assemble via a reversible pathway that includes fibril breaking and rejoining. *J. Mol. Biol.* **376**, 1116–1129
11. Griffin, M.D., Mok, M.L., Wilson, L.M., Pham, C.L., Waddington, L.J., Perugini, M.A., and Howlett, G.J. (2008) Phospholipid interaction induces molecular-level polymorphism in apolipoprotein C-II amyloid fibrils via alternative assembly pathways. *J. Mol. Biol.* **375**, 240–256
12. Stewart, C.R., Wilson, L.M., Zhang, Q., Pham, C.L., Waddington, L.J., Staples, M.K., Stapleton, D., Kelly, J.W., and Howlett, G.J. (2007) Oxidized cholesterol metabolites found in human atherosclerotic lesions promote apolipoprotein C-II amyloid fibril formation. *Biochemistry* **46**, 5552–5561
13. Ryan, T.M., Howlett, G.J., and Bailey, M.F. (2008) Fluorescence detection of a lipid-induced tetrameric intermediate in amyloid fibril formation by apolipoprotein C-II. *J. Biol. Chem.* **283**, 35118–35128
14. Ryan, T.M., Teoh, C.L., Griffin, M.D., Bailey, M.F., Schuck, P., and Howlett, G.J. (2010) Phospholipids

Enhance Nucleation but Not Elongation of Apolipoprotein C-II Amyloid Fibrils. *J. Mol. Biol.* **399**, 731–740
15. Goldsbury, C.S., Wirtz, S., Muller, S.A., Sunderji, S., Wicki, P., Aebi, U., and Frey, P. (2000) Studies on the in vitro assembly of Abeta 1-40: implications for the search for Abeta fibril formation inhibitors. *J. Struct. Biol.* **130**, 217–231
16. Jimenez, J.L., Nettleton, E.J., Bouchard, M., Robinson, C.V., Dobson, C.M., and Saibil, H.R. (2002) The protofilament structure of insulin amyloid fibrils. *Proc. Natl Acad. Sci. USA* **99**, 9196–9201
17. Chamberlain, A.K., MacPhee, C.E., Zurdo, J., Morozova-Roche, L.A., Hill, H.A., Dobson, C.M., and Davis, J.J. (2000) Ultrastructural organization of amyloid fibrils by atomic force microscopy. *Biophys. J.* **79**, 3282–3293
18. Chien, P., Weissman, J.S., and DePace, A.H. (2004) Emerging principles of conformation-based prion inheritance. *Annu. Rev. Biochem.* **73**, 617–656
19. Jones, E.M. and Surewicz, W.K. (2005) Fibril conformation as the basis of species- and strain-dependent seeding specificity of mammalian prion amyloids. *Cell* **121**, 63–72
20. Ban, T., Hamada, D., Hasegawa, K., Naiki, H., and Goto, Y. (2003) Direct observation of amyloid fibril growth monitored by thioflavin T fluorescence. *J. Biol. Chem.* **278**, 16462–16465
21. Ban, T., Hoshino, M., Takahashi, S., Hamada, D., Hasegawa, K., Naiki, H., and Goto, Y. (2004) Direct observation of Abeta amyloid fibril growth and inhibition. *J. Mol. Biol.* **344**, 757–767
22. Ban, T., Morigaki, K., Yagi, H., Kawasaki, T., Kobayashi, A., Yuba, S., Naiki, H., and Goto, Y. (2006) Real-time and single fibril observation of the formation of amyloid beta spherulitic structures. *J. Biol. Chem.* **281**, 33677–33683
23. Ban, T., Yamaguchi, K., and Goto, Y. (2006) Direct observation of amyloid fibril growth, propagation, and adaptation. *Acc. Chem. Res.* **39**, 663–670
24. Yagi, H., Ban, T., Morigaki, K., Naiki, H., and Goto, Y. (2007) Visualization and classification of amyloid beta supramolecular assemblies. *Biochemistry* **46**, 15009–15017
25. Ozawa, D., Yagi, H., Ban, T., Kameda, A., Kawakami, T., Naiki, H., and Goto, Y. (2009) Destruction of amyloid fibrils of a beta2-microglobulin fragment by laser beam irradiation. *J. Biol. Chem.* **284**, 1009–1017
26. Andersen, C.B., Yagi, H., Manno, M., Martorana, V., Ban, T., Christiansen, G., Otzen, D.E., Goto, Y., and Rischel, C. (2009) Branching in amyloid fibril growth. *Biophys. J.* **96**, 1529–1536
27. Yagi, H., Ozawa, D., Sakurai, K., Kawakami, T., Kuyama, H., Nishimura, O., Shimanouchi, T., Kuboi, R., Naiki, H., and Goto, Y. (2010) Laser-induced propagation and destruction of amyloid beta fibrils. *J. Biol. Chem.* **285**, 19660–19667
28. Naiki, H., Higuchi, K., Hosokawa, M., and Takeda, T. (1989) Fluorometric determination of amyloid fibrils in vitro using the fluorescent dye, thioflavin T1. *Anal. Biochem.* **177**, 244–249
29. Biancalana, M. and Koide, S. (2010) Molecular mechanism of Thioflavin-T binding to amyloid fibrils. *Biochim. Biophys. Acta* **1804**, 1405–1412